Interpretation of Measured Aerosol Mass Scattering Efficiency Over North America Using a Chemical Transport Model

Robyn N. C. Latimer[1*], Randall V. Martin[1,2*]

[1]Department of Physics and Atmospheric Science, Dalhousie University, Halifax, B3H 4R2
5   [2]Harvard-Smithsonian Center for Astrophysics, Cambridge, MA 02138, USA

Correspondence to: Robyn Latimer (robyn.latimer93@gmail.ca) and Randall Martin (randall.martin@dal.ca)

Abstract. Aerosol mass scattering efficiency affects climate forcing calculations, atmospheric visibility, and the interpretation of satellite observations of aerosol optical depth. We evaluated the representation of aerosol mass scattering efficiency (α_{sp}) in the GEOS-Chem chemical transport model over North America using collocated measurements of aerosol 10 scatter and mass from IMPROVE network sites between 2000-2015. We found a positive bias in mass scattering efficiency given current assumptions of aerosol size distributions and particle hygroscopicity in the model. We found that overestimation of mass scattering efficiency was most significant in dry (RH<35%) and midrange humidity (35%<RH<65%) conditions, with biases of 87% and 38%, respectively. To address these biases, we investigated assumptions surrounding the two largest contributors to fine aerosol mass, organic (OA) and secondary inorganic aerosols (SIA). Inhibiting hygroscopic 15 growth of SIA below 35% RH and decreasing the dry geometric mean radius, from 0.069 μm for SIA and 0.073 μm for OA to 0.058 μm for both aerosol types, significantly decreased the bias observed in dry conditions from 87% to 13%. Implementation of a widely used alternative representation of hygroscopic growth following κ-Kohler theory for secondary inorganic (hygroscopicity parameter κ=0.58) and organic (κ=0.10) aerosols eliminated the remaining overall bias in α_{sp}. Simulated average α_{sp} over North America increased by 12%, with larger increases of 20% to 40% in northern regions with 20 high RH and hygroscopic aerosol fractions, and decreases in α_{sp} up to 15% in the southwestern U.S. where RH is low.

1. Introduction

The interaction of atmospheric aerosols with radiation has substantial implications for the direct radiative effects of atmospheric aerosols, atmospheric visibility, and satellite retrievals of aerosol optical properties. The direct radiative effects of aerosols remain a major source of uncertainty in radiative forcing (Myhre et al., 2013). Atmospheric visibility affects the 25 appearance of landscape features, which is of particular concern in national parks and wilderness areas (Malm et al., 1994)**.** Gaining insight into the concentration and composition of atmospheric aerosols via interpretation of satellite retrievals of aerosol optical depth (AOD) also relies heavily on an understanding of the interaction of aerosols with radiation (Kahn et al., 2005). Analysis of collocated measurements of aerosol scatter, mass, and composition could offer valuable insight into aerosol optical properties.

Current chemical transport models and global circulation models often calculate atmospheric extinction due to aerosols from speciated aerosol mass concentrations using a composition and size dependent mass extinction efficiency (α_{ext}, $m^2\ g^{-1}$). Many of these models use aerosol optical and physical properties defined by the Global Aerosol Data Set (GADS), compiled from measurements and models from 1970 to 1995 (Koepke et al., 1997). The subsequent growth in long term

5   aerosol monitoring offers an exciting possibility to further improve model representation of aerosol physical and optical properties. The Interagency Monitoring of Protected Visual Environments (IMPROVE) network offers long-term collocated measurements since 1987 of particle scatter (b_{sp}), relative humidity (RH), fine particulate mass concentrations less than 10 μm (PM_{10}) and less than 2.5 μm ($PM_{2.5}$) mass as well as chemical composition at sites across the United States and Canada (Malm et al., 1994; Malm et al., 2004). These collocated measurements provide direct measurements of mass scattering

10   efficiency (α_{sp}) across North America that are useful to evaluate and improve the mass scattering efficiency currently used in models.

Several prior studies have analyzed mass scattering efficiencies. Hand et al. (2007) performed an extensive review that examined and compared mass scattering efficiencies calculated from ground based measurements from approximately 60 mostly short-term studies from 1990 to 2007. In this review, the importance of long term measurements was emphasized.

15   Malm & Hand (2007) applied IMPROVE network data between 1987-2003 to evaluate mass scattering efficiency of organic and inorganic aerosols at 21 IMPROVE sites. A couple more recent examples of short term studies of mass scattering efficiency are Titos et al. (2012) and Tao et al. (2014). Many other long-term multi-site studies have investigated aerosol optical properties (e.g. Andrews et al., 2011; Coen et al., 2013; Pandolfi et al., 2017), but few include measurements of aerosol mass concentrations and therefore do not provide information on mass scattering efficiencies. Our study builds upon

20   previous studies of mass scattering efficiency by reducing initial assumptions regarding size and hygroscopicity of inorganic and organic aerosols and by using measurements of particle speciation, mass and scatter to inform the representation of these properties. We interpret long term measurement data to obtain a representation of mass scattering efficiency that can be used across an array of conditions and locations to facilitate incorporation into chemical transport models.

Here we interpret collocated measurements of $PM_{2.5}$, PM_{10}, b_{sp} and RH from the IMPROVE network to understand

25   factors affecting the representation of mass scattering efficiency. Section 2 provides a description of IMPROVE network measurements, of the GEOS-Chem chemical transport model, and of an alternate aerosol hygroscopic growth scheme. In Section 3, we present an analysis of the current representation of mass scattering efficiency in the GEOS-Chem model, and identify changes that improve the consistency with observations. The impact of these changes on GEOS-Chem simulated mass scattering efficiency, as well as on agreement between the GEOS-Chem model and observations from the IMPROVE

30   network are described in section 4.

2. Methods

2.1 IMPROVE network measurements

The IMPROVE network (Malm et al., 1994) is a long-term monitoring program established in 1987 to monitor visibility trends in national parks and wilderness areas in the United States. The network offers collocated measurements of $PM_{2.5}$

5   speciation, $PM_{2.5}$ and PM_{10} gravimetric mass, b_{sp} and RH that we interpret to understand mass scattering efficiency.

The IMPROVE particle sampler collects $PM_{2.5}$ and PM_{10} on filters. Sampling occurs over a 24h period every third day. Collected $PM_{2.5}$ is analyzed for fine gravimetric mass, elemental concentrations (including Al, Si, Ca, Fe, Ti), ions (SO_4^{2-}, NO_3-, NO_2^-, Cl^-), and organic and elemental carbon. Collected PM_{10} undergoes gravimetric analysis for coarse mass (Malm et al., 1994).

10 Particle scatter (b_{sp}) is measured at 550 nm at a subset of IMPROVE sites using OPTEC NGN-2 open air integrating nephelometers (Malm et al., 2007). b_{sp} is measured hourly at ambient air temperature and relative humidity; all three parameters are recorded. We filter b_{sp} data to exclude measurements likely affected by meteorological interference such as fog. These conditions include an RH threshold of 95%, a maximum b_{sp} threshold of 5000 Mm^{-1} and an hourly rate of change threshold for b_{sp} of 50 Mm^{-1}, following IMPROVE filtering protocols (IMPROVE, 2004).

15 For this study, we select sites where fine aerosol mass and speciation measurements are collocated with IMPROVE nephelometers between 2000-2015. We exclude coastal sites between 2000-2005, since reliable estimates of sea salt concentrations were unavailable prior to 2005, and since sea salt can contribute significantly to b_{sp} in coastal conditions of high RH due to its highly hygroscopic nature (Lowenthal and Kumar, 2006). We use only days with coincident mass and scatter measurements. Additionally, only days with a minimum of 23 hourly measurements are used, to reduce influence of

20 meteorological interference.

Figure 1 shows at the 30 sites used in this study the average b_{sp}, PM_{10} and $PM_{2.5}$ measured between 2000-2015. Measured b_{sp} values vary by a factor of 7 with scatter below 20 Mm^{-1} across the southwest U.S., and scatter above 50 Mm^{-1} across the southeast U.S. Measured PM_{10} concentrations vary by a factor of 3 with values below 6 $\mu g\ m^{-3}$ in the west to above 14 $\mu g\ m^{-3}$ in the southeast. Measured $PM_{2.5}$ concentrations also vary by a factor of 3, with values below 3 $\mu g\ m^{-3}$ in

25 the west to above 9 $\mu g\ m^{-3}$ in the southeast.

2.2 GEOS-Chem simulation

We simulate hourly $PM_{2.5}$ and PM_{10} mass concentrations and particle scatter using the global chemical transport model GEOS-Chem (version 11.01, http://geos-chem.org). The GEOS-Chem model is driven by assimilated meteorology from the Goddard Earth Observation System (GEOS MERRA-2) of the NASA Global Modeling and Assimilation Office (GMAO).

30 Our simulation is conducted at 2° x 2.5° resolution over 47 vertical levels.

GEOS-Chem simulates detailed aerosol-oxidant chemistry (Bey et al., 2001; Park et al., 2004). The aerosol simulation includes the sulfate-nitrate-ammonium system (Park et al., 2004), primary (Park et al., 2003; Wang et al., 2014) and secondary (Pye et al., 2010) carbonaceous aerosols, mineral dust (Fairlie et al., 2007; Fairlie et al., 2010; Zhang et al., 2013) and sea salt (Jaeglé et al., 2011). Organic matter (OM) is estimated from primary organic carbon (OC) using spatially and seasonally varying OM/OC ratios at 0.1° x 0.1° resolution (Philip et al., 2014). The thermodynamic equilibrium model ISORROPIA-II (Fountoukis and Nenes, 2007), implemented by Pye et al. (2009), is used to calculate gas-aerosol partitioning. Aerosol physical and optical properties are defined by the Global Aerosol Data Set (GADS) (Koepke et al., 1997), as implemented by Martin et al. (2003), with modifications to dry size distributions (Drury et al., 2010) and dust mass partitioning (Ridley et al., 2012). Default optical parameters are given in Table A1. Total $PM_{2.5}$ is calculated following van Donkelaar et al. (2010), but at 40% RH here for consistency with the IMPROVE network gravimetric analysis in the range of 30-50% RH (Solomon et al., 2014). Particle scatter and aerosol optical depth are calculated at ambient RH based on dry species mass concentrations and aerosol physical and optical properties.

We conduct a simulation for the year 2006, to represent the period of greatest measurement density of collocated b_{sp} and PM sites over North America. We archive model fields every hour over North America. We simulate $PM_{10,}$ $PM_{2.5}$ and b_{sp}, allowing for the comparison of model mass scattering efficiency to that measured at IMPROVE network sites over North America.

2.3 Determining mass scattering efficiciency (α_{sp})

One method of determining mass scattering efficiencies from measurements involves b_{sp} measurements and particle mass concentration measurements (M_{meas}). Mass scattering efficiency of a given aerosol population can be defined as the ratio of particle scatter to mass.

$$\alpha_{sp,meas} = \frac{b_{sp,meas}}{M_{meas}} \tag{1}$$

Hourly mass scattering efficiencies are determined using collocated measurements of b_{sp} and mass concentrations from the IMPROVE network, treating IMPROVE mass concentrations as constant over each 24h sampling period. Total scatter is typically dominated by fine mode aerosols, but in certain conditions coarse dust can also make a significant contribution (White et al., 1994). Thus, measured PM_{10} mass is used in the denominator of Eq. (1).

Multiple definitions of α_{sp} exist. We define α_{sp} operationally here based on optical measurements at ambient RH, and PM measurements at controlled RH (treated as 40% RH). We compare these measured α_{sp} with calculated α_{sp} based on species specific mass scattering efficiencies ($\alpha_{GC,j}$) used in GEOS-Chem, constrained with mass concentrations (M_j) and PM_{10} mass measured by IMPROVE.

$$\alpha_{sp,calc} = \frac{b_{sp,calc}}{PM_{10,meas}} = \frac{\sum_j \alpha_{GC,j} M_j}{PM_{10,meas}} \tag{2}$$

Appendix A describes the calculation in more detail. This approach enables isolation at the mass scattering efficiencies used in GEOS-Chem from the species concentrations.

2.3 Introducing an alternate hygroscopic growth scheme

We examine for GEOS-Chem the use of a widely adopted alternate hygroscopic growth scheme, in which aerosol hygroscopic growth is defined by a single parameter, κ (Petters and Kreidenweis 2007, 2008, 2013). This representation of water uptake by aerosols was originally developed for supersaturated CCN conditions, but in recent years has been used extensively in subsaturated conditions (Dusek et al., 2011; Hersey et al., 2013).

The hygroscopic parameter κ is defined by

$$\frac{1}{a_w} = 1 + \kappa \frac{V_d}{V_w} \qquad (3)$$

where V_d is dry particulate matter volume, V_w is the water volume and a_w is water activity (Petters and Kreidenweis, 2013), which is unity for secondary inorganic aerosols (SIA) and organic aerosols (OA). The diameter growth factor (GF=D/D$_d$) can be expressed (Snider et al., 2016) as

$$GF = \left(1 + \kappa_v \frac{RH}{100-RH}\right)^{1/3} \qquad (4)$$

where D is the wet aerosol radius and D_d is the dry aerosol radius. Typically, κ_v is in the range of 0.5-0.7 for SIA (Hersey et al., 2013; Kreidenweis et al., 2008; Petters & Kreidenweis, 2007) and 0-0.2 for OA (Duplissy et al., 2011; Kreidenweis et al., 2008; Rickards et al., 2013; Snider et al., 2016).

3. Results

3.1 Understanding the current representation of α_{sp}

Figure 2 (left) shows measured vs. calculated mass scattering efficiency using GEOS-Chem default optical tables. Each point represents the average α_{sp} at an IMPROVE site over the entire sampling period. A significant correlation (r=0.96) is apparent, however a bias in α_{sp} is evident. A positive correlation between average mass scattering efficiency and RH is apparent; sites with low average RH have low average α_{sp} and vice versa.

To further investigate the RH dependence of this bias, we separate our analysis of calculated α_{sp} into 3 relative humidity groupings: 0-35% (low), 35-65% (mid) and 65-95% (high). The blue dots in Fig. 3 show calculated vs measured α_{sp} for each RH range. In the low RH case, a significant overestimation of mass scattering efficiency is apparent at most sites, with a bias of 87% indicated by the slope. In the mid RH case, overestimation of α_{sp} is less significant but still apparent with a bias of 38% indicated by the slope. At high RH, bias is weak.

To further understand the source of the bias in calculated mass scattering efficiency, we now examine calculated α_{sp} in conditions dominated by different aerosol types. Figure 4 shows in blue measured vs calculated α_{sp} using default optical

tables for conditions where $PM_{2.5}$ is dominated (>60%) by secondary inorganic aerosol, organic aerosol and dust, as well conditions where PM_{10} is dominated (>60%) by PM_{coarse} (PM_{10}-$PM_{2.5}$). The scatterplot in the SIA dominant case resembles the overall relationship shown in Fig. 2. α_{sp} is overestimated at most sites, with significant correlation (r=0.89), and a bias evident in the offset of 0.72. Where OA is the dominant component of $PM_{2.5}$, the slope is close to unity (0.99) but the large

5 offset of 0.87 $m^2 g^{-1}$ results in α_{sp} being largely overestimated. Where dust is the dominant fine aerosol, correlation is significant (r=0.89) and mass scattering efficiency is accurately calculated at the vast majority of sites, despite a prominent outlier at a site in the Columbia River Gorge, Washington. The PM_{coarse} dominant case shows significant correlation (r=0.90) and a slight tendency for overestimation of α_{sp}. As this case is not independent from the other cases, this overestimation is likely linked to the overestimation in the OA and SIA dominant cases as demonstrated below.

10   These results indicate that the bias in calculated mass scattering efficiency arises mostly due to the representation of the physical and optical properties of secondary inorganic and organic aerosols. The following will focus on improving the representation of physical and optical properties of these two aerosol types.

3.2 Changing the physical properties of SIA and OA

      Figure 5 shows mass scattering efficiency as a function of aerosol size for secondary inorganic (orange) and organic (blue)
15 aerosols for dry aerosols (solid) and aerosols at 80% RH (dashed lines) as calculated using a Mie algorithm ((Mishchenko et al., 1999). The uptake of water increases aerosol scatter, decreases aerosol density and decreases the refractive index. The increase in aerosol scatter with increasing ambient RH drives the increase in α_{sp}.

      The points in Fig. 5 represent the current mass scattering efficiency values of OA and SIA in GEOS-Chem. For dry aerosols, α_{sp}=4.4 $m^2 g^{-1}$ for OA and α_{sp}=3.2 $m^2 g^{-1}$ for SIA. In a review of ground-based estimates of aerosol mass scattering
20 efficiencies, Hand et al. (2007) found dry α_{sp} values of 2.5 $m^2 g^{-1}$ for ammonium sulfate, 2.7 $m^2 g^{-1}$ for ammonium nitrate, and 3.9 $m^2 g^{-1}$ for particulate organic matter. These values suggest that the default optical tables in GEOS-Chem currently overestimate mass scattering efficiency of SIA and OA in dry conditions. This reaffirms the overestimation of α_{sp} in dry conditions evident in the left panel of Fig. 3. As aerosol size is the strongest determinant of dry mass scattering efficiency, we begin by examining the dry sizes of SIA and OA in GEOS-Chem.

25   The current dry sizes of SIA and OA in GEOS-Chem were informed by measurements from several aircraft campaigns over eastern North America during the summer of 2004 (Drury et al., 2010) as part of the The International Consortium for Atmospheric Research on Transport and Transformation (ICARTT) (Fehsenfeld et al., 2006; Singh et al., 2006). Aerosol surface area and volume distributions fluctuate seasonally in the North Eastern U.S., with summer maxima and winter minima (Stanier et al., 2004). We divide our analysis at low RH by season, in an effort to discern a seasonal
30 pattern in the overestimation of α_{sp}.

      Figure 6 (blue) shows seasonal measured vs. calculated mass scattering efficiency in dry conditions using default optical tables (Table A1). Estimations of α_{sp} are most accurate in the summer, consistent with the dry sizes chosen by Drury

et al. (2010) which were informed by summertime size distribution measurements. The larger overestimation of α_{sp} in all other seasons, most notably in winter, is consistent with the seasonality in aerosol size distributions observed by Stanier et al. (2004).

3.2.1 Efflorescence relative humidity

5 To address the overestimation of mass scattering efficiency in dry conditions illustrated in Fig. 3 and Fig. 6, we begin by accounting for efflorescence transitions in secondary inorganic aerosols. Efflorescence phase transitions are characterized by nucleation of the crystalline phase followed by rapid evaporation of water. Field measurements have found evidence for these transitions (Martin et al., 2008). The efflorescence relative humidity (ERH) of ammonium sulfate reported in several experimental studies range from 35-40% (Ciobanu et al., 2010). Laboratory tests have shown that mixtures of sulfate-nitrate-

10 ammonium particles will undergo efflorescence when the ammonium sulfate fraction is high (Dougle et al., 1998; Martin et al., 2003). This condition is true at most global measurement sites, with the possible exception of Europe, where particles are nitrate rich (Martin et al., 2003).

We therefore define the hygroscopic growth factor for SIA as unity for RH ≤ 35%, linearly increasing between 35-40% RH from unity to $GF_{40\%}$ (calculated by Eq. (4)), and following the default (or κ-Kohler) growth curve for RH ≥ 40%.

15 Incorporating an ERH for SIA and consequently inhibiting hygroscopic growth of SIA below 35% RH significantly reduces the overestimation of mass scattering efficiency in dry conditions. In the case of default hygroscopic growth in GEOS-Chem, the overall dry bias in α_{sp} is reduced from 87% to 53%.

3.2.2 Aerosol dry size

To address the remaining overestimation of mass scattering efficiency in dry conditions we explore different dry sizes of

20 secondary inorganic and organic aerosols. Figure 7 shows the slope of the average measured vs calculated α_{sp} plot for RH<35% for dry radii ranging from 0.050 to 0.074 μm at intervals of 0.001 μm, assuming SIA and OA have the same dry size. The slope of the best fit line acts as an indicator of the appropriate dry size for each season. Sensitivity tests exploring alternative error metrics (RMSE, MSE) yielded similar results. The slope decreases steadily as dry radius is decreased in all seasons. Slope as a function of radius is nearly identical in the spring and fall, diverging slightly for the smallest sizes.

25 Using the dry radius which gives a slope of unity, we find that aerosols are largest in summer (r=0.067 μm), smallest in winter (r=0.052 μm), and in between in spring and fall (0.057 μm and 0.056 **μ**m, respectively). Averaging the sizes from all four seasons results in an annual representative dry radius of 0.058 μm.

Figure 6 (red) shows seasonal measured vs. calculated α_{sp} in dry conditions using this new representative annual geometric mean radius for SIA and OA. This change in geometric mean radius reduces the overestimation of α_{sp} in all

30 seasons, with the largest improvement in spring (slope decreases from 1.73 to 1.01) and winter (slope decreases from 1.87 to 1.16). Changes in correlation are minor.

3.2.3 Aerosol hygroscopicity

We now examine the implementation of the widely adopted κ-Kohler hygroscopic growth scheme described in section 2.3. A range of measured κ values for SIA (κ_s) and OA (κ_o) exist in the literature. We explore the range of possible κ values, using the slope of the measured vs calculated α_{sp} plot as an indicator of the appropriate values.

5   Figure 8 shows the slope of the measured vs calculated α_{sp} plot for κ values for SIA (κ_s) ranging from 0.5-0.7 and for OA (κ_o) ranging from 0.08-0.20. Slope increases steadily as κ_s and κ_o increase. A slope of unity identifies representative values of κ_s=0.58 and κ_o=0.10. These values are in the middle of the range of measured κ values (Duplissy et al., 2011; Hersey et al., 2013; Kreidenweis et al., 2008; Petters and Kreidenweis, 2007; Rickards et al., 2013).

Figure 9 shows the diameter growth factor as a function of relative humidity following κ-Kohler theory, as well as

10   GADS hygroscopic growth for both SIA and OA used in the default GEOS-Chem model. Hygroscopic growth from the Aerosol Inorganic Model (AIM) at T=298 K (Wexler and Clegg, 2002) and laboratory measurements (Wise et al., 2003) are also shown for ammonium sulfate (Snider et al., 2016). The GADS hygroscopic growth schemes used in the default GEOS-Chem simulation are characterized by larger growth at low RH and smaller growth at high RH for both secondary inorganic and organic aerosols. The κ-Kohler scheme exhibits greater consistency with both AIM and laboratory hygroscopic growth

15   for SIA.

Using the revised dry size of 0.058 μm and the κ-Kohler theory of hygroscopic growth, we calculate revised physical and optical properties for SIA and OA over a range of RH values. Table A1 contains geometric mean radius, extinction efficiency and single scattering albedo for the revised optical tables at 8 relative humidity values.

Figure 2 (right) shows the measured vs calculated mass scattering efficiency using these revised optical tables for

20   SIA and OA. The overestimation of mass scattering efficiency has been eliminated with these revised aerosol properties, with a slope of 1.00 and an offset of 0.05. Correlation remains significant at r=0.97.

Figure 4 (red) shows measured vs calculated α_{sp} in conditions dominated by different aerosol types using the revised optical tables. The overestimation of α_{sp} in SIA dominant conditions using the default optical tables has been eliminated, with a slope of 1.00 and a decreased offset (0.79 to 0.1). The large overestimation of α_{sp} that was apparent in OA

25   dominant conditions has been reduced by a factor of 2. α_{sp} remains accurately estimated at the majority of dust dominant sites, with the outlier at the Columbia River Gorge site in Washington still skewing the best fit line. The slight overestimation of α_{sp} that was present in the PM$_{coarse}$ dominant case using default optical tables has been eliminated using the revised tables (offset 0.36 to 0.03). Moderate increases in correlation coefficients are apparent in all cases except for the SIA dominant case, where it decreased by 0.02.

30   Figure 3 (red) shows measured vs calculated α_{sp} using revised optical tables. The overestimation in α_{sp} has been significantly reduced in the low RH case (slope=1.87 to slope=1.13) and in the mid RH case (slope=1.38 to slope=0.98)

compared to when default optical tables were used. The slight overestimation in high RH conditions present in the default case has also been reduced, as shown by the decreased offset (0.84 to 0.65).

3.3 Changes in GEOS-Chem simulated α_{sp}

Here, we examine how these changes to aerosol properties impact both GEOS-Chem simulation of mass scattering
5   efficiency over North America and the fit between modeled and measured α_{sp} at IMPROVE sites. These simulations rely on GEOS-Chem simulations of aerosol composition using GEOS RH fields.

Figure 10 shows the relative and absolute change in mass scattering efficiency when switching from the default to revised optical tables. Continental mean α_{sp} increased by 12%. Increases in α_{sp} range from 20-40% in northeastern regions of North America, corresponding to an increase of 1-3 $m^2 g^{-1}$. These larger changes reflect the higher RH and SIA fractions.
10   Decreases in α_{sp} of up to 15% or -0.5 $m^2 g^{-1}$ are found in the southwest where RH is low and mineral dust dominates.

Figure 11 shows GEOS-Chem annual average mass scattering efficiency using default (top) and revised (bottom) optical tables over North America for the year 2006. The overlaying circles represent average measured α_{sp} at IMPROVE network sites for the year 2006, and the outer rings show the coincident simulated α_{sp} for each site. We exclude sites within 1° of the coast where sea-salt affects α_{sp}, as well as sites where elevation differs from average gridbox elevation by more
15   than 1500 meters. These criteria result in a decrease from 24 to 19 in the number of sites available for the analysis in 2006.

Using default optical tables, simulated continental mean α_{sp} is 5.4 $m^2 g^{-1}$. A maximum α_{sp} of 10 $m^2 g^{-1}$ occurs in British Columbia, and a minimum α_{sp} of 1.7 $m^2 g^{-1}$ occurs in the southwest United States. Using revised optical tables, simulated continental mean α_{sp} is 6.2 $m^2 g^{-1}$, with a maximum of 12.2 $m^2 g^{-1}$ in the northwest, and a minimum of 1.5 $m^2 g^{-1}$ in the southwest.
20   Figure 12 (left) shows coincident measured vs simulated mass scattering efficiency at the 19 IMPROVE sites, using default optical tables. Correlation is significant (r=0.88), but a bias in simulated α_{sp} is apparent (slope=0.83). Simulated α_{sp} is notably biased low at sites in the southeastern United States where average α_{sp} is largest, and simulated α_{sp} is notably biased high at sites in the southwestern United States where average mass scattering efficiency is lowest. Sites with lowest average RH correspond to those with the lowest average mass scattering efficiency and vice versa. The tendency of mass scattering
25   efficiency to be overestimated at low RH reflects the tendency that was originally seen in Fig. 4.

Figure 12 (right) shows coincident measured vs simulated α_{sp} using revised optical tables. Correlation remains significant (r=0.89), and a decrease in bias is evident from the increase in slope (0.83 to 0.90) and decrease in offset (0.47 to 0.10). Most sites now lie closer to the 1:1 line. The overestimation of simulated α_{sp} in the southwest, where RH is low, has been reduced or eliminated at all sites.

3.4 Comparison with AERONET measurements

Appendix B investigates changes to simulated AOD, and compares measured and simulated AOD at AERONET sites. Although large relative increases upwards of 60% in average AOD are evident in large parts of northern high-latitudes where absolute AOD is small, absolute AOD generally changes by less than 0.1 (Fig. B1). Comparisons with AERONET AOD

5   reveal that the revised optical properties slightly improve the simulation of AOD worldwide (slope decreases from 1.08 to 0.99) despite the large influence of other factors (e.g. ambient aerosol concentrations) upon AOD.

4. Conclusions

The current representation of mass scattering efficiency in the GEOS-Chem global chemical transport model was evaluated using collocated ground-based measurements of particle mass, speciation, scatter and relative humidity from the IMPROVE

10   network.

Calculated mass scattering efficiency had a positive bias using default physical and optical properties used in the GEOS-Chem model. This bias was most significant when $PM_{2.5}$ mass was dominated by secondary inorganic (SIA) or organic aerosols (OA). $PM_{2.5}$ dust and coarse particulate matter were accurately represented at the majority of IMPROVE sites.

15   Relative humidity played an important role in the severity of the bias in mass scattering efficiency. Mean α_{sp} was overestimated by 87% in dry conditions (RH<35%). This bias was largest in the winter (87%) and smallest in the summer (29%). Implementing an efflorescence relative humidity for SIA and thus inhibiting hygroscopic growth below 35% RH decreased the dry bias by 34%. An annual representative dry geometric mean radius of 0.058 μm for SIA and OA decreased the dry mass scattering efficiency of these aerosols, and subsequently further reduced the bias in dry conditions to 13%.

20   κ-Kohler theory was implemented for the hygroscopic growth of SIA and OA, which is characterized by smaller growth factors at low RH and larger growth factors at high RH compared to default growth factors in GEOS-Chem. κ values of 0.58 for SIA and 0.10 for OA eliminated the overall bias in calculated mass scattering efficiency.

These changes to SIA and OA optical tables resulted in a continental mean increase in GEOS-Chem simulated mass scattering efficiency of 12%. Northeastern regions of North America exhibited the largest increases (20-40%) due to high

25   RH and SIA fractions, while southwestern regions of the continent exhibited decreases in α_{sp} of up to 15% due to low RH and high dust fractions. These changes to the GEOS-Chem optical tables improved the fit between measured and simulated mass scattering efficiency at IMPROVE sites, reflected in the changes to the slope (0.83 to 0.90) and the offset (0.47 to 0.10).

Future work should examine the implications of these changes for satellite-derived estimates of fine particulate

30   matter that depend on the relationship of AOD with $PM_{2.5}$. Future work should also expand analysis of the representation of mass scattering efficiency, by incorporating measurements from other ground based measurement networks such as the

Surface PARTiculate MAtter network (SPARTAN), which provides measurements of particulate mass, speciation and scatter in populated regions worldwide (Snider et al., 2015; Snider et al., 2016). Such comparisons may also be useful to evaluate and improve prognostic simulations of aerosol size (Mann et al., 2010; Spracklen et al., 2005; Trivitayanurak et al., 2008; Yu and Luo, 2009) .

5 **Appendix A**

A.1 b_{sp} and α_{sp} calculations in GEOS-Chem

In GEOS-Chem, surface level b_{sp} is calculated using model particle mass concentrations and local relative humidity, as well as predefined mass densities and aerosol optical properties for each aerosol component following:

$$b_{sp} = \sum_{species,i} \frac{\frac{3}{4}*\left(\frac{R_{w,i}}{R_{d,i}}\right)^2 *M_{d,i}*Q_{w,i}*SSA_{w,i}}{\rho_{d,i}*R_{d,i}} \tag{A1}$$

10 where ρ_d is the dry particle mass density, R_w is the effective radius (defined as the ratio of the third to second moment of an aerosol size distribution), R_d is the dry effective radius, M_d is the dry surface level mass concentration, Q_w is the extinction efficiency, and SSA_w is the single scattering albedo. Parameters with the subscript w indicate values at ambient RH. Species included in this calculation are SO_4^{2-}, NH_4^+, NO_3^-, BC, OM and fine and coarse dust and sea salt.

Dividing Eq. (5) by total surface level PM_{10} results in the following equation for mass scattering efficiency

15 $$\alpha_{sp} = \frac{B_{sp}}{PM_{10}} = \sum_{species,i} \frac{\frac{3}{4}*\left(\frac{R_{w,i}}{R_{d,i}}\right)^2 *\frac{M_{d,i}}{PM_{10}}*Q_{w,i}*SSA_{w,i}}{\rho_{d,i}*R_{d,i}} \tag{A2}$$

The effective radius, extinction efficiency and single scattering albedo in Eq. (A1) and (A2) are obtained from GEOS-Chem optical tables for the ambient RH values measured by IMPROVE. Dry mass density ρ_d is specified for each aerosol species in GEOS-Chem (Table A2). $M_{d,i}$ and PM_{10} are obtained from IMPROVE network measurements of aerosol mass and composition. α_{sp} calculated by Eq. (A2) is compared to α_{sp} directly measured by the IMPROVE network.

20 Mass scattering efficiency is dependent on particle density, refractive index and particle size. Mass scattering efficiency is typically most dependent on aerosol size, which is dictated by both the dry size distribution chosen to represent a given aerosol species, and by the hygroscopic growth scheme used to represent aerosol water uptake for hydrophilic species.

A.2 Incorporating IMPROVE Network Measurements

25 The IMPROVE network measures every three days $PM_{2.5}$ mass and speciation and PM_{10} mass. The IMPROVE particle sampler consists of four independent modules with separate inlets and pumps. The first three modules (A, B and C) collect only fine particulate matter ($PM_{2.5}$), while the 4th module (D) collects both fine and coarse particles (PM_{10}). Module A collects $PM_{2.5}$ on a Teflon filter, which undergoes gravimetric analysis for total $PM_{2.5}$ mass and x-ray florescence for

elemental concentrations (including Al, Si, Ca, Fe, Ti). The nylon filter in module B undergoes ion chromatography analysis for SO_4^{2-}, NO_3^-, NO_2^- and Cl^-. Module C contains a quartz filter that is analyzed for organic and elemental carbon via thermal optical reflectance. The Teflon filter in module D undergoes gravimetric analysis for PM_{10} mass (Malm et al., 1994; Malm et al., 2004). Prior to gravimetric analysis, filters A and D undergo equilibration at 30-50% RH and 20-25 °C for several
5   minutes (Solomon et al., 2014).

The GEOS-Chem model partitions OM into hydrophilic and hydrophobic fractions, so the same is done for OM measured by IMPROVE. OM in remote regions tends to be highly oxidized, and oxidation level of organics has been shown to positively correlate with hygroscopicity (Duplissy et al., 2011; Jimenez et al., 2009; Ng et al., 2010). We treat measured OM as 90% hydrophilic, due to the rural nature of IMPROVE sites. EC is treated as 50% hydrophilic. As speciation of
10 coarse material is unavailable, we treat all coarse material as crustal in origin, an assumption that may breakdown at coastal sites. We partition fine and coarse dust measured by the IMPROVE network into the GEOS-Chem size bins using the dust particle size distribution (PSD) described by Zhang et al. (2013).

Appendix B

The *Ae*rosol *Ro*botics *Net*work (AERONET) is a long-term network of ground based sun photometers that provides
15 continuous, cloud-screened measurements of aerosol optical depth (AOD) at several fixed wavelengths in the visible and near infrared (Holben et al., 1998). The calculation of AOD in GEOS-Chem is performed using simulated mass concentrations of aerosol species and mass extinction efficiencies, summed over all vertical layers. Our analysis of mass scattering efficiency can therefore be extended globally by comparing GEOS-Chem calculated AOD to AOD measured at AERONET sites. During our simulation year of 2006, AERONET consisted of 231 sites across the globe.
20 Here we examine how the changes to SIA and OA properties impact GEOS-Chem simulated AOD globally. Figure B1 shows the relative (top) and absolute (bottom) changes in AOD. Global mean AOD increases by 18%. Relative changes in AOD are most pronounced in Northern regions where mean relative humidity is high, with increases in simulated AOD ranging from 50-90%. Decreases in AOD between 0-20% are present in most of the southern hemisphere, in part due to the lower average RH. Absolute changes in AOD show a similar tendency, with slight increases in AOD of up to 0.2 in northern
25 regions, and slight decreases of up of -0.09 in southern regions. An exception to this is seen over parts of China, where AOD increases by 0.5 due to the elevated SIA and OA concentrations.

Figure B2 shows coincident measured (inner circles) and simulated (outer rings) AOD for the year 2006 using default optical tables (top) and revised optical tables (bottom). We exclude sites within 1° of the coast, as well as sites where elevation differs from average gridbox elevation by more than 1500 meters. We also exclude sites where average $PM_{2.5}$ is
30 dominated by dust (dust/$PM_{2.5}$>0.6), to focus on the representation of the optical properties of SIA and OA. Across the globe, we see that AOD is both over and underestimated. AOD is overestimated at most sites in Africa, with the most

notable overestimation at the site in Nigeria. AOD is moderately overestimated at sites in Australia. Underestimation of AOD occurs at most sites in South America, as well as at sites in southern North America and southern Asia.

Figure B3 shows coincident measured vs simulated AOD at AERONET sites for default (left) and revised (right) optical tables. The correlation coefficient (r=0.80 to r=0.78) changes insignificantly, while the slope decreases from 1.08 to 0.99 when switching to the revised optical tables. In summary, the revised optical properties developed for North America slightly improve the representation of AOD at the global scale, despite the large influence of other factors (e.g. ambient aerosol concentrations) upon AOD.

Data Availability

IMPROVE network data for 2000-2015 can be accessed at http://vista.cira.colostate.edu/Improve/improve-data/.

Acknowledgements

Research described in this article was conducted under contract to the Health Effects Institute (HEI), an organization jointly funded by the United States Environmental Protection Agency (EPA) (Assistance Award No. R-82811201) and certain motor vehicle and engine manufacturers. The contents of this article do not necessarily reflect the views of HEI, or its sponsors, nor do they necessarily reflect the views and policies of the EPA or motor vehicle and engine manufacturers.

IMPROVE is a collaborative association of state, tribal, and federal agencies, and international partners. US Environmental Protection Agency is the primary funding source, with contrcting and research support from the National Park Service. The Air Quality Group at the University of California, Davis is the central analytical laboratory, with ion analysis provided by Research Triangle Institute, and carbon analysis provided by Desert Research Institute.

We thank Environment and Climate Change Canada for providing nephelometer data at the site in Egbert, Ontario.

References

Andrews, E., Ogren, J. A., Bonasoni, P., Marinoni, A., Cuevas, E., Rodríguez, S., Sun, J. Y., Jaffe, D. A., Fischer, E. V., Baltensperger, U., Weingartner, E., Coen, M. C., Sharma, S., Macdonald, A. M., Leaitch, W. R., Lin, N. H., Laj, P., Arsov, T., Kalapov, I., Jefferson, A. and Sheridan, P.: Climatology of aerosol radiative properties in the free troposphere, Atmos. Res., 102(4), 365–393, doi:10.1016/j.atmosres.2011.08.017, 2011.

Bey, I., Jacob, D. J., Yantosca, R. M., Logan, J. A., Field, B. D., Fiore, A. M., Li, Q.-B., Liu, H.-Y., Mickley, L. J. and Schultz, M. G.: Global Modeling of Tropospheric Chemistry with Assimilated Meteorology: Model Description and

doi:10.1029/2006JD007829, 2006.

Fountoukis, C. and Nenes, A.: ISORROPIA II: a computationally efficient thermodynamic equilibrium model for K –H 2 O aerosols, Atmos. Chem. Phys. Atmos. Chem. Phys., 7, 4639–4659, doi:10.5194/acp-7-4639-2007, 2007.

Hand, J. L. and Malm, W. C.: Review of aerosol mass scattering efficiencies from ground-based measurements since 1990, J. Geophys. Res. Atmos., 112(16), doi:10.1029/2007JD008484, 2007.

Hersey, S. P., Craven, J. S., Metcalf, A. R., Lin, J., Lathem, T., Suski, K. J., Cahill, J. F., Duong, H. T., Sorooshian, A., Jonsson, H. H., Shiraiwa, M., Zuend, A., Nenes, A., Prather, K. A., Flagan, R. C. and Seinfeld, J. H.: Composition and hygroscopicity of the Los Angeles Aerosol: CalNex, J. Geophys. Res. Atmos., 118(7), 3016–3036, doi:10.1002/jgrd.50307, 2013.

Holben, B. N., Eck, T. F., Slutsker, I., Tanré, D., Buis, J. P., Setzer, A., Vermote, E., Reagan, J. A., Kaufman, Y. J., Nakajima, T., Lavenu, F., Jankowiak, I. and Smirnov, A.: AERONET—A Federated Instrument Network and Data Archive for Aerosol Characterization, Remote Sens. Environ., 66(1), 1–16, doi:10.1016/S0034-4257(98)00031-5, 1998.

Jaeglé, L., Quinn, P. K., Bates, T. S., Alexander, B. and Lin, J. T.: Global distribution of sea salt aerosols: New constraints from in situ and remote sensing observations, Atmos. Chem. Phys., 11(7), 3137–3157, doi:10.5194/acp-11-3137-2011, 2011.

Jimenez, J. L., Canagaratna, M. R., Donahue, N. M., Prevot, a. S. H., Zhang, Q., Kroll, J. H., DeCarlo, P. F., Allan, J. D., Coe, H., Ng, N. L., Aiken, a. C., Docherty, K. S., Ulbrich, I. M., Grieshop, A. P., Robinson, a. L., Duplissy, J., Smith, J. D., Wilson, K. R., Lanz, V. a., Hueglin, C., Sun, Y. L., Tian, J., Laaksonen, A., Raatikainen, T., Rautiainen, J., Vaattovaara, P., Ehn, M., Kulmala, M., Tomlinson, J. M., Collins, D. R., Cubison, M. J., Dunlea, J., Huffman, J. A., Onasch, T. B., Alfarra, M. R., Williams, P. I., Bower, K., Kondo, Y., Schneider, J., Drewnick, F., Borrmann, S., Weimer, S., Demerjian, K., Salcedo, D., Cottrell, L., Griffin, R., Takami, a., Miyoshi, T., Hatakeyama, S., Shimono, A., Sun, J. Y., Zhang, Y. M., Dzepina, K., Kimmel, J. R., Sueper, D., Jayne, J. T., Herndon, S. C., Trimborn, a. M., Williams, L. R., Wood, E. C., Middlebrook, A. M., Kolb, C. E., Baltensperger, U., Worsnop, D. R., Dunlea, E. J., Huffman, J. A., Onasch, T. B., Alfarra, M. R., Williams, P. I., Bower, K., Kondo, Y., Schneider, J., Drewnick, F., Borrmann, S., Weimer, S., Demerjian, K., Salcedo, D., Cottrell, L., Griffin, R., Takami, a., Miyoshi, T., Hatakeyama, S., Shimono, A., Sun, J. Y., Zhang, Y. M., Dzepina, K., Kimmel, J. R., Sueper, D., Jayne, J. T., Herndon, S. C., Trimborn, a. M., Williams, L. R., Wood, E. C., Middlebrook, A. M., Kolb, C. E., Baltensperger, U., Worsnop, D. R., Dunlea, J., Huffman, J. A., et al.: Evolution of Organic Aerosols in the Atmosphere, Science (80-.)., 326(5959), 1525–1529, doi:10.1126/science.1180353, 2009.

Kahn, R. A., Gaitley, B. J., Martonchik, J. V., Diner, D. J., Crean, K. A. and Holben, B.: Multiangle Imaging Spectroradiometer (MISR) global aerosol optical depth validation based on 2 years of coincident Aerosol Robotic Network (AERONET) observations, J. Geophys. Res. D Atmos., 110(10), 1–16, doi:10.1029/2004JD004706, 2005.

Koepke, P., Hess, M., Schult, I. and Shettle, E. P.: Global Aerosol Data Set., 1997.

Kreidenweis, S. M., Petters, M. D. and DeMott, P. J.: Single-parameter estimates of aerosol water content, Environ. Res. Lett., 3(3), 35002, doi:10.1088/1748-9326/3/3/035002, 2008.

Lowenthal, D. and Kumar, N.: Light scattering from sea-salt aerosols at interagency monitoring of protected visual

environments (IMPROVE) sites, J. Air Waste Manag., 56(5), 636–642, doi:10.1080/10473289.2006.10464478, 2006.

Malm, C., Sisler, J. F. and Cahill, A.: Spatial and seasonal trends in particle concentration and optical extinction in the United States, , 99, 1347–1370, 1994.

Malm, W. C.: Spatial and monthly trends in speciated fine particle concentration in the United States, J. Geophys. Res.,
5   109(D3), D03306, doi:10.1029/2003JD003739, 2004.

Malm, W. C. and Hand, J. L.: An examination of the physical and optical properties of aerosols collected in the IMPROVE program, Atmos. Environ., 41(16), 3407–3427, doi:10.1016/j.atmosenv.2006.12.012, 2007.

Mann, G. W., Carslaw, K. S., Spracklen, D. V., Ridley, D. A., Manktelow, P. T., Chipperfield, M. P., Pickering, S. J. and Johnson, C. E.: Description and evaluation of GLOMAP-mode: A modal global aerosol microphysics model for the UKCA
10   composition-climate model, Geosci. Model Dev., 3(2), 519–551, doi:10.5194/gmd-3-519-2010, 2010.

Martin, R. V.: Global and regional decreases in tropospheric oxidants from photochemical effects of aerosols, J. Geophys. Res., 108(D3), 4097, doi:10.1029/2002JD002622, 2003.

Martin, S. T., Schlenker, J. C., Malinowski, A. and Hung, H.: Crystallization of atmospheric sulfate-nitrate-ammonium particles, , 30(21), 1–4, doi:10.1029/2003GL017930, 2003.

15   Martin, S. T., Rosenoern, T., Chen, Q. and Collins, D. R.: Phase changes of ambient particles in the Southern Great Plains of Oklahoma, Geophys. Res. Lett., 35(22), 1–5, doi:10.1029/2008GL035650, 2008.

Mishchenko, M. I., Dlugach, J. M., Yanovitskij, E. G. and Zakharova, N. T.: Bidirectional reflectance of flat, optically thick particulate layers: An efficient radiative transfer solution and applications to snow and soil surfaces, J. Quant. Spectrosc. Radiat. Transf., 63(2–6), 409–432, doi:10.1016/S0022-4073(99)00028-X, 1999.

20   Ng, N. L., Canagaratna, M. R., Zhang, Q., Jimenez, J. L., Tian, J., Ulbrich, I. M., Kroll, J. H., Docherty, K. S., Chhabra, P. S., Bahreini, R., Murphy, S. M., Seinfeld, J. H., Hildebrandt, L., Donahue, N. M., Decarlo, P. F., Lanz, V. A., Prévôt, A. S. H., Dinar, E., Rudich, Y. and Worsnop, D. R.: Organic aerosol components observed in Northern Hemispheric datasets from Aerosol Mass Spectrometry, Atmos. Chem. Phys., 10(10), 4625–4641, doi:10.5194/acp-10-4625-2010, 2010.

Pandolfi, M., Alados-arboledas, L., Andrade, M., Backman, J., Baltensperger, U., Bonasoni, P., Bukowiecki, N., Coen, C.,
25   Conil, S., Coz, E., Crenn, V., Dudoitis, V., Eleftheriadis, K., Favez, O., Fetfatzis, P., Fiebig, M., Ginot, P., Gysel, M., Henzing, B., Hoffer, A., Holubova, A., Kalapov, I., Kalivitis, N., Kouvarakis, G., Kristensson, A., Kulmala, M., Lihavainen, H., Lunder, C., Luoma, K., Lyamani, H., Mihalopoulos, N., Moerman, M., Dowd, C. O., Petit, J., Pichon, J. M., Prokopciuk, N., Putaud, J., Sciare, J., Sellegri, K., Stamenov, D. B., Swietlicki, E., Titos, G., Tuch, T., Tunved, P., Ulevicius, V., Vaishya, A., Virkkula, A., Vratolis, S., Weingartner, E., Wiedensohler, A. and Laj, P.: Discussion started : 13 October 2017
30   Manuscript under review for journal Atmos . Chem . Phys . Discussion started : 13 October 2017 c Author (s) 2017 . CC BY 4 . 0 License ., , (October), 2017.

Park, R. J.: Sources of carbonaceous aerosols over the United States and implications for natural visibility, J. Geophys. Res., 108(D12), 4355, doi:10.1029/2002JD003190, 2003.

Park, R. J., Jacob, D. J., Field, B. D., Yantosca, R. M. and Chin, M.: Natural and transboundary pollution influences on

sulfate-nitrate-ammonium aerosols in the United States: Implications for policy, J. Geophys. Res. D Atmos., 109(15), doi:10.1029/2003JD00473, 2004.

Petters, M. D. and Kreidenweis, S. M.: A single parameter representation of hygroscopic growth and cloud\ncondensation nucleus activity, Atmos. Chem. Phys., 1961–1971, doi:10.5194/acp-7-1961-2007, 2007.

5   Petters, M. D. and Kreidenweis, S. M.: A single parameter representation of hygroscopic growth and cloud condensation nucleus activity-Part 3: Including surfactant partitioning, Atmos. Chem. Phys., 13(2), 1081–1091, doi:10.5194/acp-13-1081-2013, 2013.

Philip, S., Martin, R. V., Pierce, J. R., Jimenez, J. L., Zhang, Q., Canagaratna, M. R., Spracklen, D. V., Nowlan, C. R., Lamsal, L. N., Cooper, M. J. and Krotkov, N. A.: Spatially and seasonally resolved estimate of the ratio of organic mass to

10   organic carbon, Atmos. Environ., 87, 34–40, doi:10.1016/j.atmosenv.2013.11.065, 2014.

Pye, H. O. T., Liao, H., Wu, S., Mickley, L. J., Jacob, D. J., Henze, D. J. and Seinfeld, J. H.: Effect of changes in climate and emissions on future sulfate-nitrate-ammonium aerosol levels in the United States, J. Geophys. Res. Atmos., 114(1), 1–18, doi:10.1029/2008JD010701, 2009.

Pye, H. O. T., Chan, A. W. H., Barkley, M. P. and Seinfeld, J. H.: Global modeling of organic aerosol: The importance of

15   reactive nitrogen (NOx and NO3), Atmos. Chem. Phys., 10(22), 11261–11276, doi:10.5194/acp-10-11261-2010, 2010.

Rickards, A. M. J., Miles, R. E. H., Davies, J. F., Marshall, F. H. and Reid, J. P.: Measurements of the sensitivity of aerosol hygroscopicity and the κ parameter to the O/C ratio, J. Phys. Chem. A, 117(51), 14120–14131, doi:10.1021/jp407991n, 2013.

Ridley, D. A., Heald, C. L. and Ford, B.: North African dust export and deposition: A satellite and model perspective, J.

20   Geophys. Res. Atmos., 117(2), 1–21, doi:10.1029/2011JD016794, 2012.

Singh, H. B., Brune, W. H., Crawford, J. H., Jacob, D. J. and Russell, P. B.: Overview of the summer 2004 Intercontinental Chemical Transport Experiment-North America (INTEX-A), J. Geophys. Res. Atmos., 111(24), doi:10.1029/2006JD007905, 2006.

Snider, G., Weagle, C. L., Martin, R. V., Van Donkelaar, A., Conrad, K., Cunningham, D., Gordon, C., Zwicker, M.,

25   Akoshile, C., Artaxo, P., Anh, N. X., Brook, J., Dong, J., Garland, R. M., Greenwald, R., Griffith, D., He, K., Holben, B. N., Kahn, R., Koren, I., Lagrosas, N., Lestari, P., Ma, Z., Vanderlei Martins, J., Quel, E. J., Rudich, Y., Salam, A., Tripathi, S. N., Yu, C., Zhang, Q., Zhang, Y., Brauer, M., Cohen, A., Gibson, M. D. and Liu, Y.: SPARTAN: A global network to evaluate and enhance satellite-based estimates of ground-level particulate matter for global health applications, Atmos. Meas. Tech., 8(1), 505–521, doi:10.5194/amt-8-505-2015, 2015.

30   Snider, G., Weagle, C. L., Murdymootoo, K. K., Ring, A., Ritchie, Y., Stone, E., Walsh, A., Akoshile, C., Anh, N. X., Balasubramanian, R., Brook, J., Qonitan, F. D., Dong, J., Griffith, D., He, K., Holben, B. N., Kahn, R., Lagrosas, N., Lestari, P., Ma, Z., Misra, A., Norford, L. K., Quel, E. J., Salam, A., Schichtel, B., Segev, L., Tripathi, S., Wang, C., Yu, C., Zhang, Q., Zhang, Y., Brauer, M., Cohen, A., Gibson, M. D., Liu, Y., Martins, J. V., Rudich, Y. and Martin, R. V.: Variation in global chemical composition of PM2.5: emerging results from SPARTAN, Atmos. Chem. Phys., 16(15), 9629–9653,

doi:10.5194/acp-16-9629-2016, 2016.

Solomon, P. A., Crumpler, D., Flanagan, J. B., Jayanty, R. K. M., Rickman, E. E. and McDade, C. E.: U.S. National PM2.5 Chemical Speciation Monitoring Networks-CSN and IMPROVE: Description of Networks., J. Air Waste Manage. Assoc., 64(12), 1410–38, doi:10.1080/10962247.2014.956904, 2014.

5   Spracklen, D. V., Pringle, K. J., Carslaw, K. S., Chipperfield, M. P. and Mann, G. W.: A global off-line model of size-resolved aerosol microphysics: I. Model development and prediction of aerosol properties, Atmos. Chem. Phys., 5(8), 2227–2252, doi:10.5194/acp-5-2227-2005, 2005.

Stanier, C. O., Khlystov, A. Y. and Pandis, S. N.: Ambient aerosol size distributions and number concentrations measured during the Pittsburgh Air Quality Study (PAQS), Atmos. Environ., 38(20), 3275–3284, doi:10.1016/j.atmosenv.2004.03.020,
10   2004.

Tao, J., Zhang, L., Ho, K., Zhang, R., Lin, Z., Zhang, Z., Lin, M., Cao, J., Liu, S. and Wang, G.: Impact of PM 2 . 5 chemical compositions on aerosol light scattering in Guangzhou — the largest megacity in South China, Atmos. Res., 135–136, 48–58, doi:10.1016/j.atmosres.2013.08.015, 2014.

Titos, G., Foyo-Moreno, I., Lyamani, H., Querol, X., Alastuey, A. and Alados-Arboledas, L.: Optical properties and
15   chemical composition of aerosol particles at an urban location: An estimation of the aerosol mass scattering and absorption efficiencies, J. Geophys. Res. Atmos., 117(4), 1–12, doi:10.1029/2011JD016671, 2012.

Trivitayanurak, W., Adams, P. J., Spracklen, D. V. and Carslaw, K. S.: Tropospheric aerosol microphysics simulation with assimilated meteorology: Model description and intermodel comparison, Atmos. Chem. Phys., 8(12), 3149–3168, doi:10.5194/acp-8-3149-2008, 2008.

20   Wang, Q., Jacob, D. J., Spackman, J. R., Perring, A. E., Schwarz, J. P., Moteki, N., Marais, E. A., Ge, C., Wang, J. and Barrett, S. R. H.: Global budget and radiative forcing of black carbon aerosol : Constraints from pole-to-pole (HIPPO) observations across the Paci fi c, , 119, 195–206, doi:10.1002/2013JD020824, 2014.

Wexler, A. S. and Clegg, S. L.: Atmospheric aerosol models for systems including the ions H + , NH 4 + , Na + , SO 4 2− , NO 3 − , Cl − , Br − , and H 2 O, J. Geophys. Res., 107(D14), 4207, doi:10.1029/2001JD000451, 2002.

25   White, W. H., Macias, E. S., Nininger, R. C. and Schorran, D.: Size-resolved measurements of light scattering by ambient particles in the southwestern U.S.A., Atmos. Environ., 28(5), 909–921, doi:10.1016/1352-2310(94)90249-6, 1994.

Wise, M. E.: Hygroscopic growth of ammonium sulfate/dicarboxylic acids, J. Geophys. Res., 108(D20), 4638, doi:10.1029/2003JD003775, 2003.

Yu, F. and Luo, G.: Simulation of particle size distribution with a global aerosol model: Contribution of nucleation to aerosol
30   and CCN number concentrations, Atmos. Chem. Phys., 9(20), 7691–7710, doi:10.5194/acp-9-7691-2009, 2009.

Zhang, L., Kok, J. F., Henze, D. K., Li, Q. and Zhao, C.: Improving simulations of fine dust surface concentrations over the western United States by optimizing the particle size distribution, Geophys. Res. Lett., 40(12), 3270–3275, doi:10.1002/grl.50591, 2013.
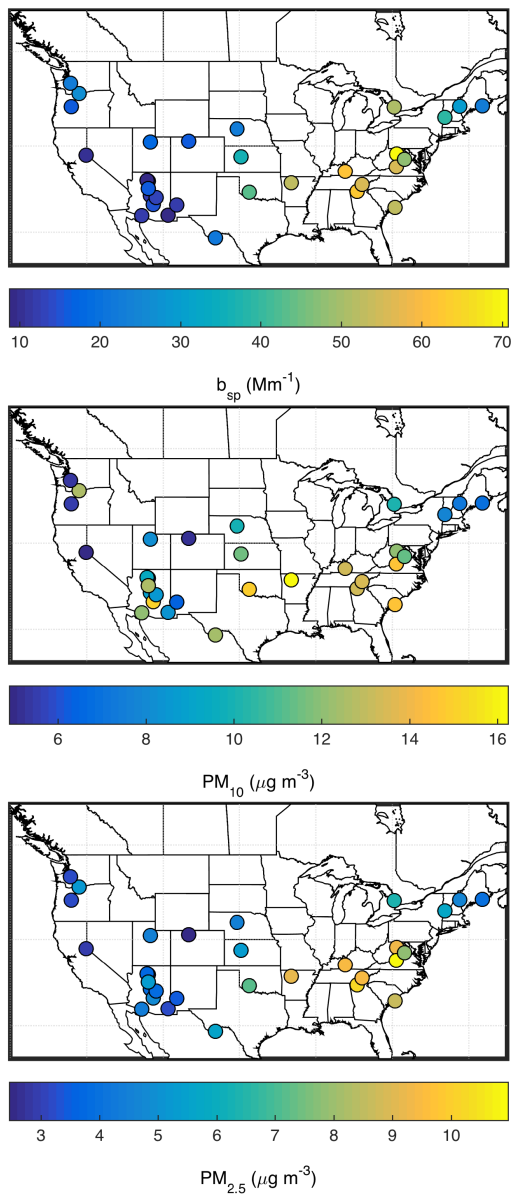
Figure 1: Map of IMPROVE sites with collocated scatter (b_{sp}), PM$_{10}$ and PM$_{2.5}$ measurements in North America between 2000-2015. Overlaying circles represent average collocated b_{sp} (top), PM$_{10}$ (middle) and PM$_{2.5}$ (bottom).
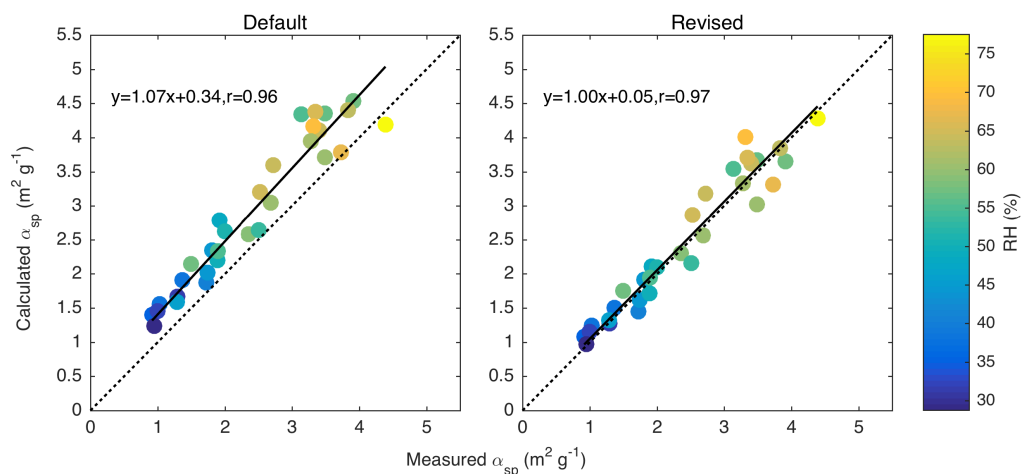
Figure 2: Average measured vs calculated α_{sp} at IMPROVE sites using GEOS-Chem default optical tables and revised optical tables. The color of each point corresponds to the average relative humidity at the site. The 1:1 line is black. Slope, offset and correlation coefficient are inset.
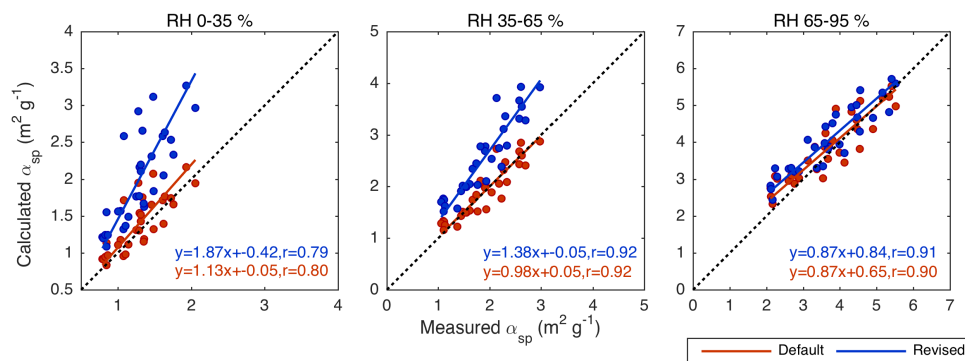
Figure 3: Average measured versus calculated α_{sp} at IMPROVE sites using GEOS-Chem default and revised optical tables for measurements taken in 0-35 % RH, 35-65 % RH and 65-95 % RH conditions. The 1:1 line is black. Slope, offset and correlation coefficient are inset.
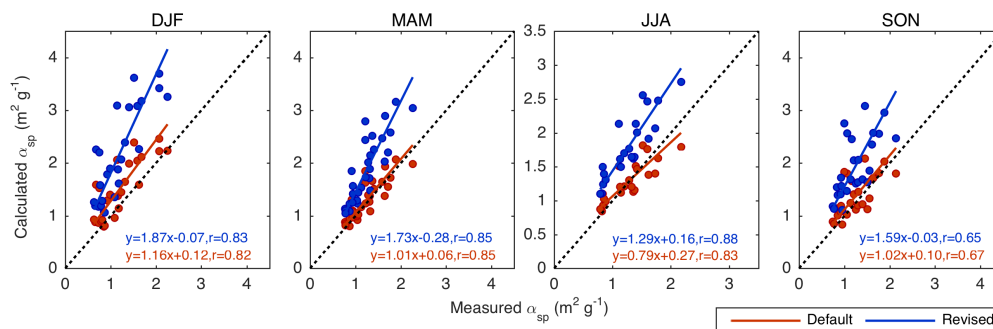
Figure 4: Average measured versus calculated α_{sp} at IMPROVE sites using GEOS-Chem default and revised optical tables using measurements taken in SIA dominant conditions, OA dominated conditions, Dust dominant conditions and PM$_{coarse}$ dominated conditions. The 1:1 line is black. Slope, offset and correlation coefficient are inset.
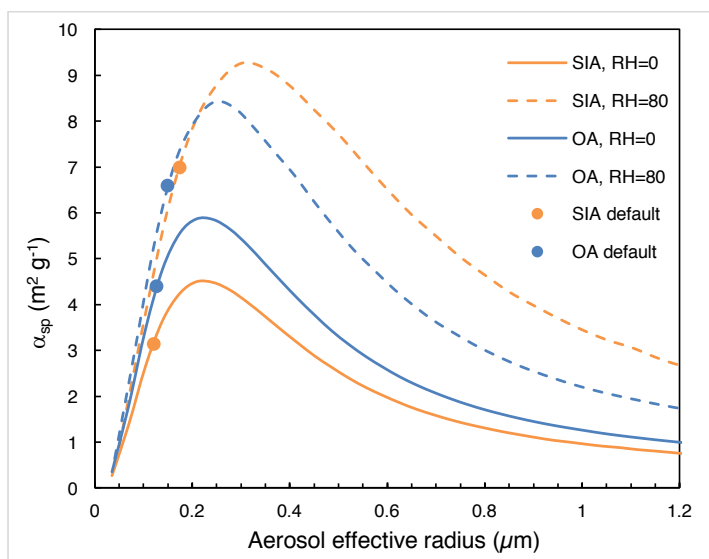
Figure 5: Mass scattering efficiency (α_{sp}) as a function of aerosol effective radius for organic aerosol and secondary inorganic aerosol. Solid lines show α_{sp} for dry aerosol (RH=0%), dashed lines show α_{sp} for aqueous aerosols (RH=80%). Points represent the default size in GEOS-Chem.
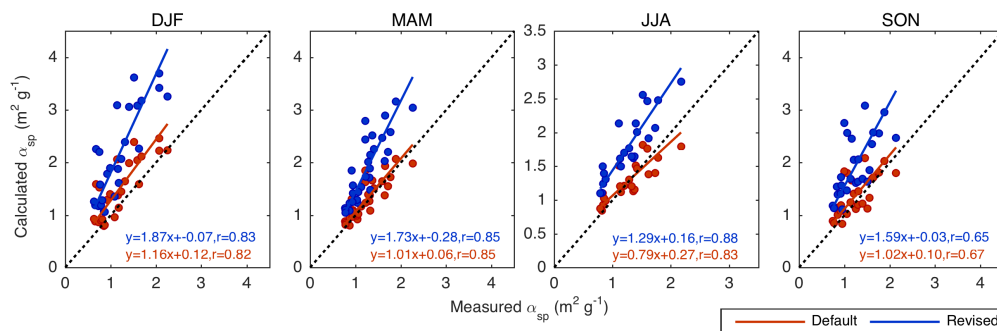
Figure 6: Average measured versus calculated α_{sp} at IMPROVE sites using GEOS-Chem default and revised optical tables for measurements taken in dry conditions (RH<35 %) in winter, spring, summer and fall. The 1:1 line is black. Slope, offset and correlation coefficient are inset.
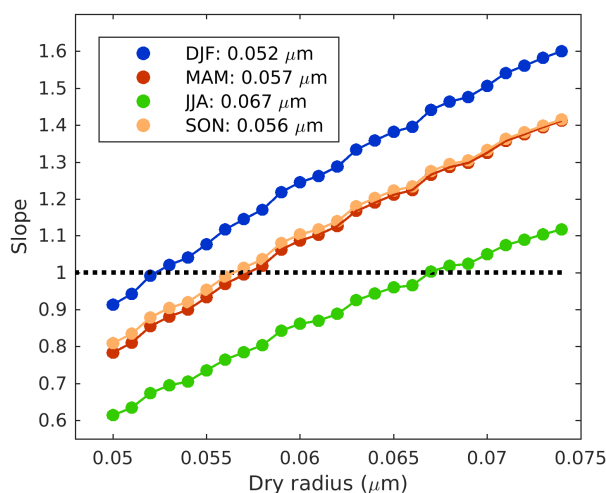
Figure 7: Slope of measured vs. calculated α_{sp} plot versus dry geometric mean aerosol radius, by season. Winter (DJF) is in blue, spring (MAM) in red, summer (JJA) in green and fall (SON) in orange. The line Slope=1 is shown in black. Numbers in the legend represent the dry radius for which slope=1 for each season.
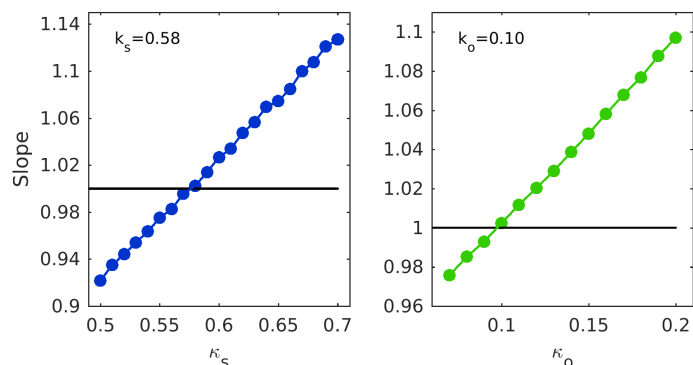
Figure 8: Slope of measured vs. calculated α_{sp} plot as a function of κ_s (left) and κ_o (right). The line slope=1 is shown in black. κ_s and κ_o values for which slope=1 are inset.
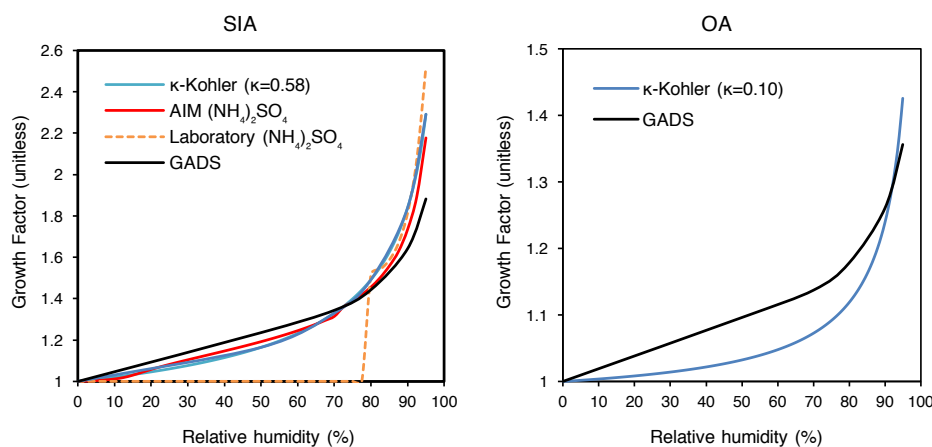
5   **Figure 9: Hygroscopic growth factor curves for SIA(left) and OA (right). GADS (Global Aerosol Data Set) hygroscopic growth from empirical data and κ-Kohler hygroscpic growth are shown for both SIA and OA. For ammonium sulfate, AIM (Aerosol Inorganic Model) hygroscopic growth at T=298 K and laboratory hygroscopic growth with a deliquesence point of RH=80 % are also shown.**
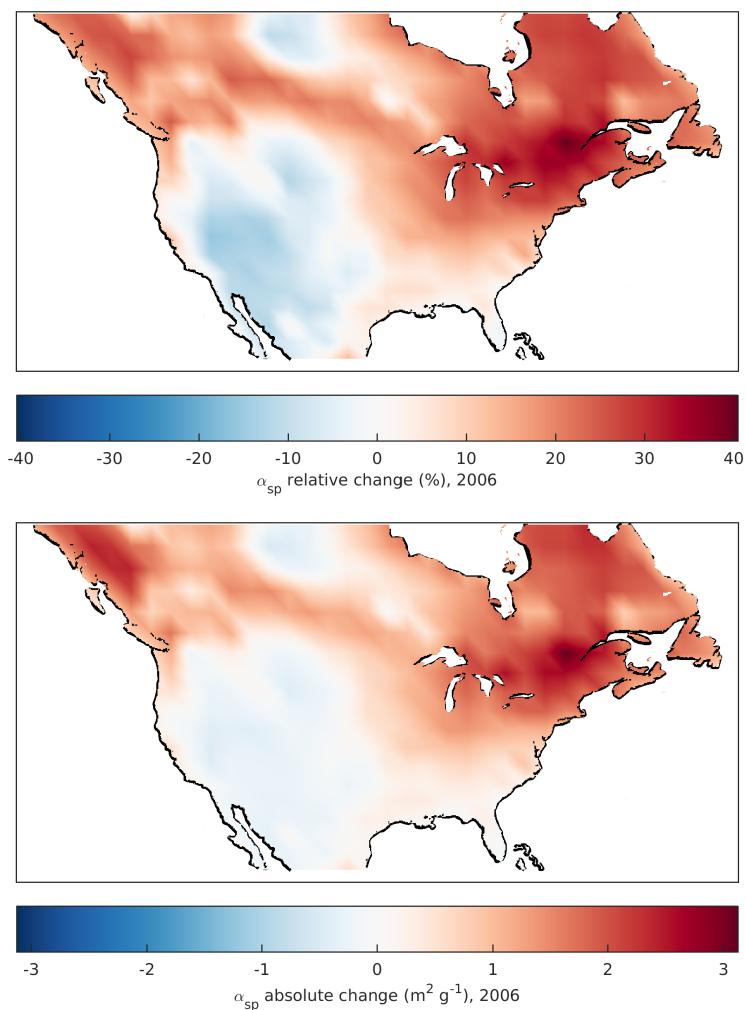
Figure 10: Average relative and absolute change in GEOS-Chem mass scattering efficiency over North America for the year 2006
5   **after implementing revised optical tables for SIA and OA.**

Figure 11: GEOS-Chem annual average mass scattering efficiency for the year 2006 using default and revised size and hygroscopicity for SIA and OA. Overlaying inner circles represent annual averages of α_{sp} at IMPROVE network sites for the year 2006. Outer rings represent coincident average simulated α_{sp}.
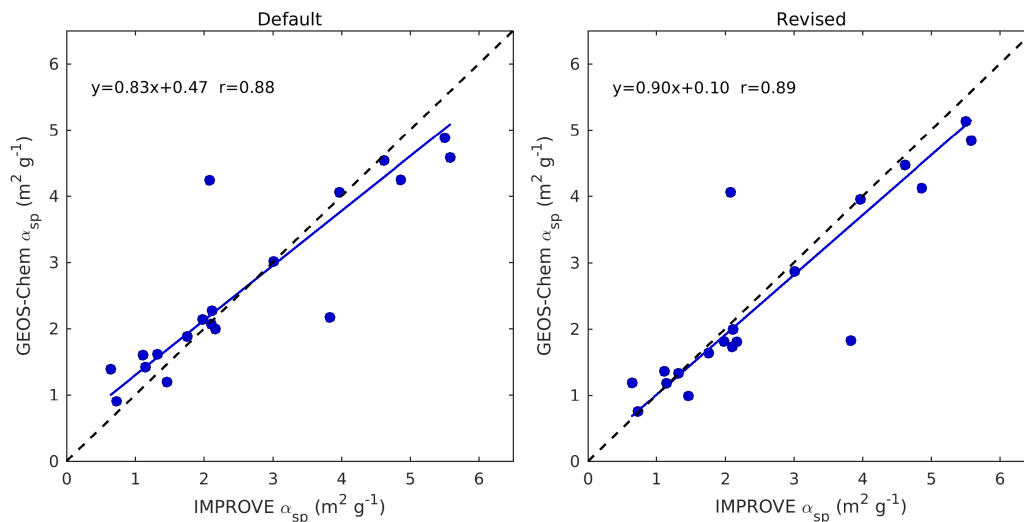
Figure 12: Coincident simulated versus measured average mass scattering efficiency for the year 2006, using default and revised optical tables. Slope, offset and correlation coefficient are inset.
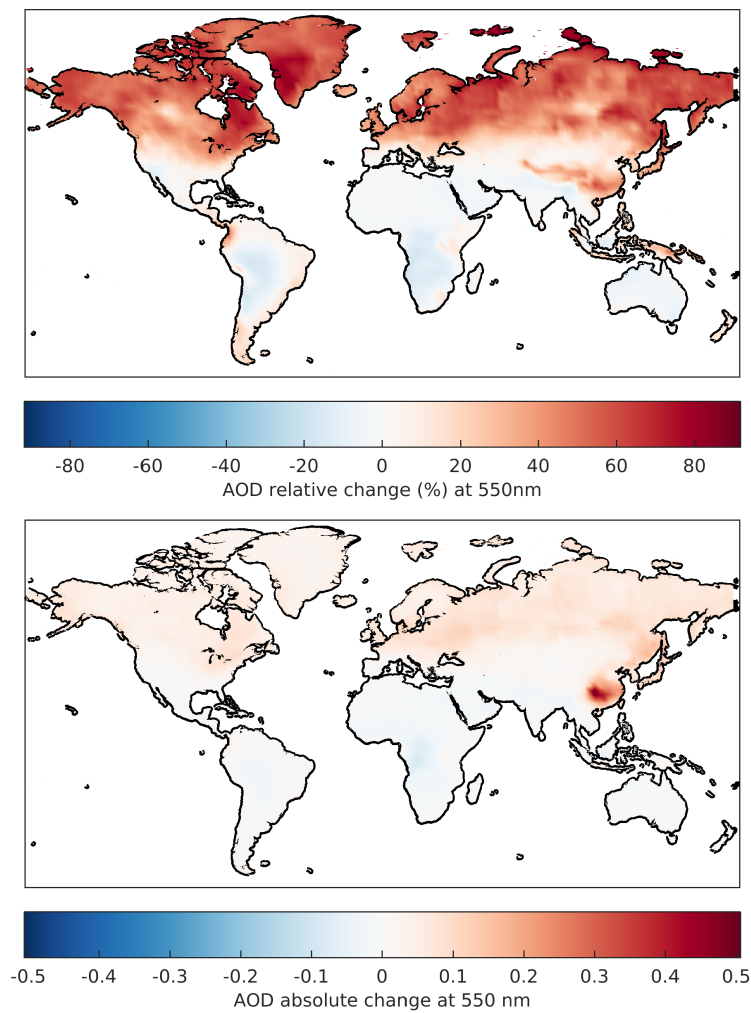
Figure B1: Average relative and absolute change in GEOS-Chem aerosol optical depth at 550 nm globally for the year 2006 after implementing revised optical tables for SIA and OA.
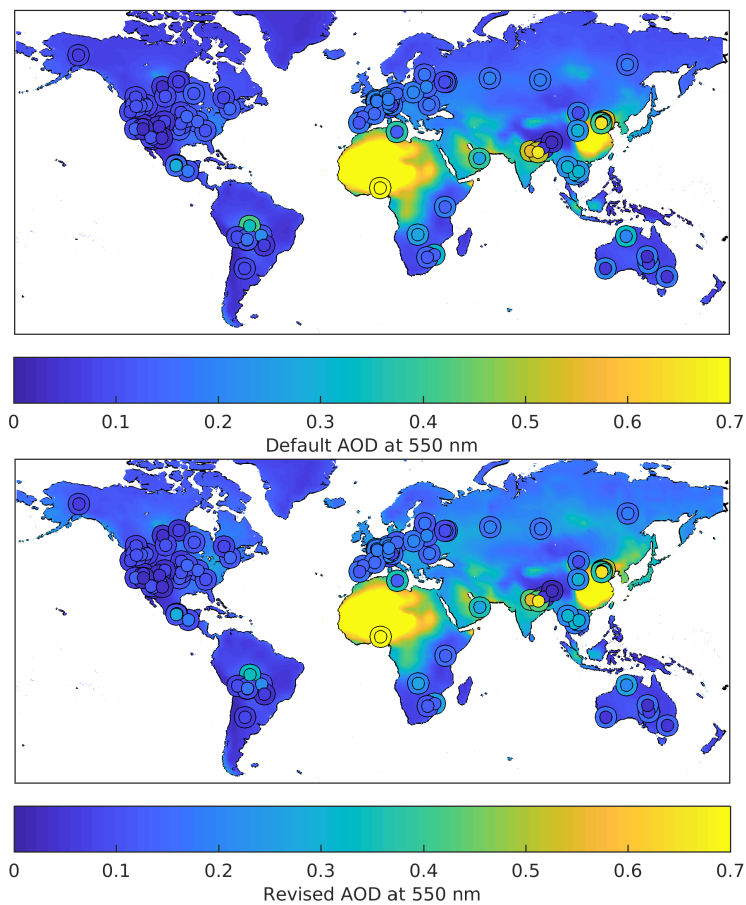
Figure B2: Global comparison for the year 2006 of AERONET AOD (inner circles) and GEOS-Chem coincident simulated AOD (outer rings) using default optical tables.
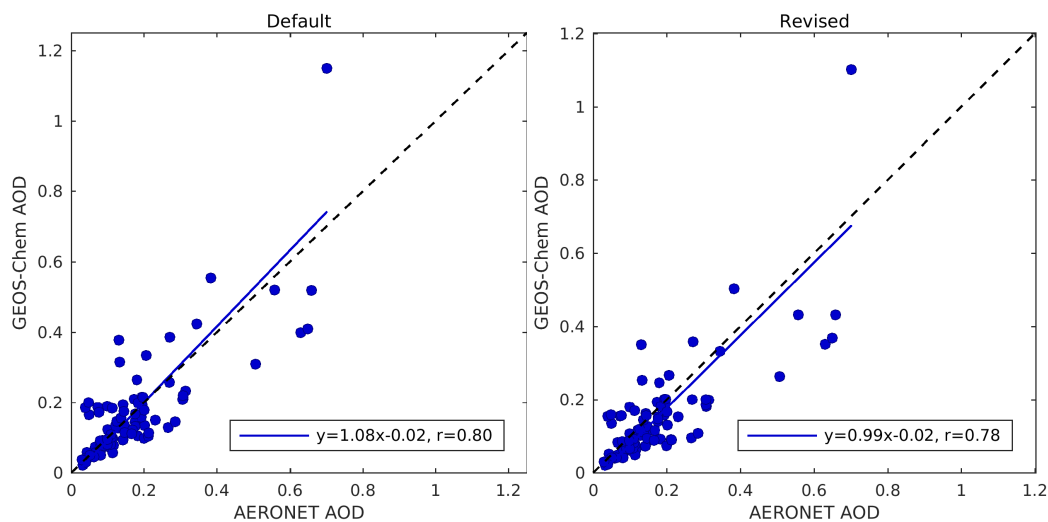
Figure B.3 Coincident simulated versus measured AOD at 550 nm at AERONET sites for the year 2006, using default and revised sizes and hygroscopicity. Slope, offset and correlation coefficient are inset. The 1:1 line is shown in black.

Aerosol	RH	Default				Revised (κ_s=0.58, κ_o=0.10)			
		r_g (μm)	r_{eff} (μm)	Q	SSA	r_g (μm)	r_{eff} (μm)	Q	SSA
SIA	0	0.069	0.121	0.902	0.965	0.058	0.101	0.603	0.959
	35	0.081	0.141	0.965	0.975	0.065	0.112	0.638	0.968
	50	0.086	0.149	0.992	0.979	0.068	0.117	0.653	0.972
	70	0.093	0.163	1.062	0.983	0.077	0.134	0.734	0.980
	80	0.100	0.174	1.137	0.986	0.087	0.150	0.835	0.986
	90	0.114	0.198	1.301	0.991	0.107	0.185	1.095	0.993
	95	0.131	0.227	1.517	0.994	0.133	0.231	1.470	0.996
	99	0.175	0.304	1.272	0.993	0.225	0.391	2.541	0.999
OA	0	0.073	0.127	1.007	0.966	0.058	0.101	0.603	0.959
	35	0.078	0.135	0.965	0.972	0.059	0.103	0.608	0.965
	50	0.080	0.139	0.947	0.975	0.060	0.104	0.610	0.963
	70	0.083	0.145	0.947	0.978	0.063	0.108	0.622	0.966
	80	0.086	0.149	0.955	0.980	0.065	0.113	0.639	0.970
	90	0.092	0.159	0.990	0.984	0.073	0.125	0.696	0.977
	95	0.099	0.171	1.053	0.988	0.084	0.144	0.811	0.985
	99	0.117	0.203	1.273	0.993	0.132	0.223	1.463	0.996

Table A1: Default and revised aerosol size and optical properties for SIA and OA at 550 nm at 8 relative humidity values. Columns indicate geometric mean radius (r_g), effective radius (r_{eff}), extinction efficiency (Q), and single scattering albedo (SSA).

Component	r_g (μm)	σ	ρ_d (g/cm^3)
Sulfate/Nitrate/Ammonium	0.070	1.6	1.7
Organic Carbon	0.073	1.6	1.3
Black Carbon	0.020	1.6	1.8
Sea-salt (fine)	0.085	1.5	2.2
Sea-salt (coarse)	0.401	1.8	2.2
Brown Carbon	0.073	1.6	1.3
Dust 1 a-d	0.030-0.170	2.2	2.5
Dust 2	0.265	2.2	2.65
Dust 3	0.530	2.2	2.65
Dust 4	0.845	2.2	2.65

Table A2: Current microphysical properties of each aerosol species in GEOS-Chem. r_g represents the dry geometric mean radius (μm) and σ the geometric standard deviation of the lognormal size distributions assumed for each species. ρ_d represents the dry mass densities of each species (g/cm^3).